The role of photon self-absorption on the H (n= 2) density determination by means of VUV emission spectroscopy and TDLAS in low pressure plasmas

Frederik Merk, Roland Friedl, Stefan Briefi, Caecilia Fröhler-Bachus, Ursel Fantz

Angaben zur Veröffentlichung / Publication details:

Merk, Frederik, Roland Friedl, Stefan Briefi, Caecilia Fröhler-Bachus, and Ursel Fantz. 2021. "The role of photon self-absorption on the H (n= 2) density determination by means of VUV emission spectroscopy and TDLAS in low pressure plasmas." Plasma Sources Science and Technology 30: 065013. https://doi.org/10.1088/1361-6595/abc93d.

PAPER • **OPEN ACCESS**

The role of photon self-absorption on the H (n = 2) density determination by means of VUV emission spectroscopy and TDLAS in low pressure plasmas

To cite this article: F Merk *et al* 2021 *Plasma Sources Sci. Technol.* **30** 065013

OPEN ACCESS
IOP Publishing
Plasma Sources Science and Technology
Plasma Sources Sci. Technol. **30** (2021) 065013 (8pp)
https://doi.org/10.1088/1361-6595/abc93d

The role of photon self-absorption on the H (n=2) density determination by means of VUV emission spectroscopy and TDLAS in low pressure plasmas

F Merk[1,*], R Friedl[2], S Briefi[1], C Fröhler-Bachus[2] and U Fantz[1,2]

[1] Max-Planck-Institut für Plasmaphysik, Boltzmannstraße 2, 85748 Garching, Germany
[2] AG Experimentelle Plasmaphysik, Universität Augsburg, Universitätsstraße 2, 86153 Augsburg, Germany

E-mail: frederik.merk@ipp.mpg.de

Received 4 August 2020, revised 22 October 2020
Accepted for publication 10 November 2020
Published 15 June 2021

Abstract

The H ($n = 2$) atomic density determination by means of vacuum ultra-violet (VUV) emission spectroscopy of the Lyman-α line in laboratory low pressure plasmas is strongly affected by self-absorption of emitted photons inside the plasma leading to an underestimation of this density. A correction of the densities obtained from VUV emission spectroscopy measurements is performed by using the escape factor method. The corrections applied can reach orders of magnitude even in low pressure plasmas. Assumptions on the spatial distribution of emitting and absorbing particles as well as on the corresponding line profiles have to be made. Consequently, additional measurements are performed, which raises the requirement of a benchmark of the applied correction procedure. In contrast, tunable diode laser absorption spectroscopy (TDLAS) on the Balmer-α line is a direct measurement of the H ($n = 2$) density and is thus suitable for a benchmark. For the ICP under consideration, H ($n = 2$) densities obtained via TDLAS are near 3×10^{15} m^{-3} whereas uncorrected VUV emission spectroscopy gives values in the range of roughly 10^{13} m^{-3} depending on pressure and applied RF power. The calculated escape factors are on the order of 2–8 $\times$ 10^{-3}. An excellent agreement with TDLAS is observed by applying them to the results of the VUV emission spectroscopy.

Keywords: absorption spectroscopy, self-absorption, VUV emission spectroscopy, hydrogen plasma

(Some figures may appear in colour only in the online journal)

1. Introduction

Spectroscopy on hydrogen plasmas resulting in the evaluation of excited state densities of atoms or molecules can be used as a tool for the determination of various plasma parameters [1]. Often performed in combination with plasma modelling, this can give access to parameters such as the electron temperature and density [2] or particle species and hence insight into the plasma chemistry [3, 4].

Concerning the determination of the H ($n \geqslant 3$) densities, usually optical emission spectroscopy (OES) on the Balmer transitions is used. Regarding the H ($n = 2$) density $n_{\mathrm{H}(n=2)}$, vacuum ultra-violet (VUV) emission spectroscopy on the

* Author to whom any correspondence should be addressed.

Lyman-α line at 121.6 nm can be performed. However, an absolute intensity calibrated VUV spectrometer is required for this purpose, whereas the availability of secondary radiation standards and the technical realization are challenging. Additionally, the Lyman-α transition is a resonant transition terminating on the hydrogen ground state and hence prone to re-absorption, which means the plasma is opaque for these photons. This self-absorption influences the Lyman-α emissivity measurement strongly. The problem of self-absorption is already dealt with for a long time (see e.g. [5]) and methods to correct for the opacity of the plasma have been developed. A widely used technique is the correction of the measured line emissivity using the line escape factors Θ_{L}. The calculation and use of escape factors is for example described in [6–9]. However, when calculating the correction factors, assumptions over the spatial distribution of H ground state and $n = 2$ atoms have to be made and, in addition, the Lyman-α emission and absorption line profiles have to be considered which is related to assumptions on the temperature of H atoms in the plasma. Beyond that, the input parameters required for the calculation (i.e. H atom density and temperature) have to be determined experimentally which requires further diagnostics in addition to the VUV emission spectrometer. Considering these aspects, a careful benchmark of the calculated escape factors for the correction procedure of the H ($n = 2$) density via VUV emission spectroscopy is highly desired.

A diagnostic method for the $n_{\mathrm{H}(n=2)}$ determination, which avoids the problem of self-absorption and is therefore suitable for a benchmark, is absorption spectroscopy on the H_α line. Here, photons with wavelengths around 656.3 nm are irradiated on the plasma to be absorbed by H ($n = 2$) atoms and from the amount of absorbed light the density of that species can be deduced. In the case of a (tunable diode) laser as photon source, this technique is known as tunable diode laser absorption spectroscopy (TDLAS), a diagnostic which is widely used for various species both in research and industrially [10, 11]. Since the spectral linewidth of the laser output radiation is usually much smaller than the half-width of the H_α line profile, the profile is accessible additionally. An application of TDLAS to the $n_{\mathrm{H}(n=2)}$ measurement is for example given in [4].

The aim of this work is to perform a benchmark of an implemented calculation of line escape factors. For this, both diagnostics are applied in a planar ICP. This experiment is further equipped with various diagnostics allowing for the required input values for the Θ_{L} calculations. The benchmark of the Θ_{L} values is performed by comparing $n_{\mathrm{H}(n=2)}$ determined by means of TDLAS and VUV emission spectroscopy under various experimental conditions.

2. Experimental setup and applied diagnostics

2.1. The planar ICP

The experimental setup can be seen in figure 1 as a CAD explosion graphic. It consists of a cylindrical vessel made of stainless steel with an inner diameter of 15 cm and a height of 10 cm. The vessel is equipped with four rectangular quartz windows and four vacuum flanges. A pump system

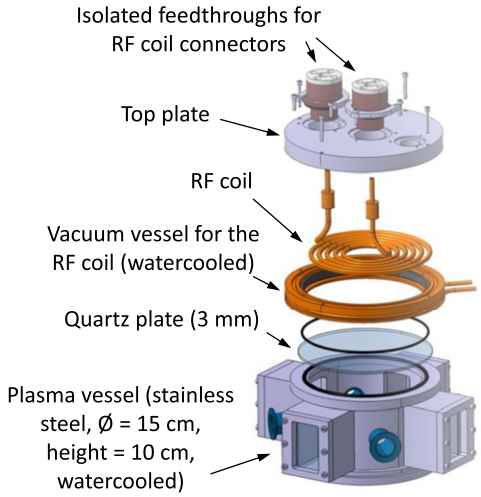

Figure 1. CAD explosion graphic of the experimental setup.

is connected and provides a background pressure of 10^{-4} Pa. The working gas is fed into the vessel via flow controllers. The working gas pressure is maintained via pumping rate adjustment using a spool valve and measured via a capacitive pressure gauge.

As ICP antenna, a planar coil with 5.5 windings is used. It is located above the plasma vessel inside a separately pumped region which is separated from the plasma vessel by a thin quartz plate to improve the power coupling to the plasma. The coil consists of a copper tube with a diameter of 6 mm which is cooled by water flowing through the tube. The coil is connected to a 2 MHz RF generator via a matching network. The generator can deliver up to 2 kW of RF power.

The investigations shown in this work are carried out at pressures between 2 Pa and 10 Pa at variable RF power between 700 W and 1000 W. The efficiency at which power is transferred into the plasma varies depending on the applied RF power and pressure inside the vessel. Therefore, the total amount of power P_{Plasma} that is transferred to the plasma is determined using the method described in [12]. Hereafter, the stated power values are always to be understood as the power coupled to the plasma.

2.2. Langmuir probe and OES

A movable Langmuir probe system is installed at the experiment. It is attached to one of the vacuum flanges. Using this system, electron temperature T_{e} and electron density n_{e} profiles can be measured across the diameter of the vessel.

OES is performed using an intensity calibrated spectrometer (*Princeton Instruments*: Acton SpectraPro 2750). Its apparatus profile is a Gaussian with a full width at half maximum between 18 and 20 pm in the wavelength range between 500 and 700 nm. The transitions investigated in this work are the Balmer lines α to δ and the Fulcher-α transition $\left(\mathrm{d}^3\Pi_u \rightarrow \mathrm{a}^3\Sigma_g^+\right)$ of molecular hydrogen located in the wavelength region between 590 nm and 650 nm. Using the method described in [13], the rotational temperature of molecular hydrogen is determined which is also corresponding to the translational temperature of H_2 denoted as T_{H_2}.

Further, the measured data is evaluated using the collisional radiative (CR) models Yacora H and Yacora H_2 [2]. These models solve the balance equations (including self-absorption effects) for all considered states of H and H_2 resulting in state resolved densities. The H atom density n_H can be obtained by comparing the measured OES data (Balmer lines α to δ and Fulcher-α transition) to the result of the CR models while varying the input parameters of the model n_H, n_e and T_e until the obtained absolute line emissivities and line ratios are matched. To validate the result, the corresponding n_e and T_e values are compared to the ones measured by Langmuir probe. In the model, the input parameter n_H is treated as the H atom ground state density (i.e. $n_{H(n=1)}$). However, looking at the determined n_H values (above 3×10^{19} m^{-3}, see section 3) in comparison to the determined $n_{H(n=2)}$ values (around 3×10^{15} m^{-3}, see section 3), it is a reasonable assumption that the determined n_H is indeed the overall H atom density. Therefore, $n_{H(n=1)}$ and n_H are treated as equal in the following. All parameters obtained by means of OES represent values averaged over the line of sight.

2.3. Vacuum UV emission spectroscopy

For the investigations on the Lyman-α line, a VUV spectrometer (*McPherson*: Model 225) equipped with a solar-blind photomultiplier tube (*EMR*: 51F-08-18) is used. The spectrometer is attached to one of the vacuum flanges on the opposite side of the Langmuir probe and is pumped separately down to a pressure of 10^{-4} Pa during plasma operation. The spectrometer is absolutely intensity calibrated in the wavelength range between 46 nm and 300 nm. As a radiation standard below 116.5 nm a high current hollow cathode lamp was used. For the Lyman-α region, special care was taken and a deuterium arc lamp was applied as radiation standard. Details on the full calibration procedure can be found in [14].

To obtain $n_{H(n=2)}$ from the Lyman-α emissivity $\epsilon_{Ly-\alpha}$, a correction for self-absorption has to be performed. This is done by applying the escape factor method according to [6]:

$$n_{H(n=2)} = \frac{\epsilon_{Ly-\alpha}}{A_{21}\Theta_L}. \tag{1}$$

A_{21} is the Einstein coefficient for spontaneous emission of the Lyman-α line and Θ_L is the corresponding *line escape factor*. The Einstein coefficient that is used here, is the effective coefficient for the Lyman-α transition which also considers the meta-stable $2^2S_{1/2}$ state when calculating $n_{H(n=2)}$ with above formula. For this, the population of the $n = 2$ fine structure sub-states according to their degeneracies g_i is assumed.

For a line of sight with length l (= 15 cm in the conducted experiments), which resembles the horizontal extent of the plasma, Θ_L is given by [15]

$$\Theta_L = \frac{\int_0^l \int_{\text{line}} J_\lambda(\lambda, x') \cdot \exp\left(-\int_{x'}^{l} \kappa(\lambda, x'')\mathrm{d}x''\right) \mathrm{d}\lambda\ \mathrm{d}x'}{\int_0^l \int_{\text{line}} J_\lambda(\lambda, x')\mathrm{d}\lambda\ \mathrm{d}x'}. \tag{2}$$

Here, $J_\lambda(\lambda, x')$ is the Lyman-α spectral emission coefficient denoting the power per unit volume and solid angle emitted due to photons in the infinitesimal wavelength interval around λ. It is given by [15]

$$\begin{aligned} J_\lambda(\lambda, x) &= n_{H(n=2)}(x)\frac{A_{21}hc}{4\pi\lambda_{21}}P^{\text{em}}_{\text{line}}(\lambda) \\ &= \epsilon_{Ly-\alpha}(x)\frac{hc}{4\pi\lambda_{21}}P^{\text{em}}_{\text{line}}(\lambda), \end{aligned} \tag{3}$$

where $P^{\text{em}}_{\text{line}}(\lambda)$ denotes the emission line profile of the Lyman-α line and λ_{21} is the corresponding emission wavelength. Further, $\kappa(\lambda, x'')$ corresponds to the Lyman-α absorption coefficient and is given by the Ladenburg relation [16]

$$\kappa(\lambda, x'') = n_{H(n=1)}(x'')\frac{g_{n=2}}{g_{n=1}}\frac{\lambda_{21}^4 A_{21}}{8\pi c} \cdot P^{\text{abs}}_{\text{line}}(\lambda). \tag{4}$$

Here, $g_{n=2}$ and $g_{n=1}$ are the statistical weights of the $n = 2$ and the ground state in atomic hydrogen, respectively, c corresponds to the speed of light in vacuum and $P^{\text{abs}}_{\text{line}}(\lambda)$ denotes the Lyman-α absorption line profile.

Over all, the value of Θ_L thus depends on the spatial distribution of both H ($n = 1$) and H ($n = 2$) atoms and the Lyman-α line profiles for both emission and absorption. The spatial distribution of hydrogen ground state atoms is assumed to be constant. This assumption can be justified by the long lifetime of hydrogen atoms in combination with a long free path length compared to the plasma dimensions allowing for a homogeneous distribution. The absolute value is given by n_H which is determined as described in section 2.2. However, a constant spatial profile does not hold for H ($n = 2$) atoms due to their short lifetime. Since the main H ($n = 2$) atom population mechanism is given by the electron impact excitation of ground state H atoms, it is assumed, that $n_{H(n=2)}$ roughly follows the excitation given by the corresponding spatial n_e and T_e distributions. In case of n_e, that was found to have the shape of a Bessel profile, whereas T_e was found to be approximately constant over the vessel diameter. The Lyman-α line profile is given by the sum of the two fine structure lines which can be seen in table 1. Further, the table contains the transition wavelength and the Einstein coefficient of the corresponding transition. The line broadening for emission and absorption depends on the temperatures $T_{H(n=2)}$ and $T_{H(n=1)}$, respectively, which are assumed to be equal and thus, also the two line profiles are assumed to be equal. Experimental data reinforcing this assumption are discussed in section 3.1. The common temperature is depicted as T_H and its determination by means of TDLAS is described in section 2.5. A complete summary of the parameters that are necessary for the escape factor calculation and the way they are obtained can be found in table 2.

Table 1. Wavelengths and transition probabilities of the allowed dipole transitions between $n = 2$ and $n = 1$ states of atomic hydrogen (Lyman-α transition) [17].

Transition ($k \leftrightarrow i$)	Wavelength (nm)	A_{ik} (s^{-1})
$1^2S_{1/2} \leftrightarrow 2^2P_{3/2}$	121.5668	6.2648×10^8
$1^2S_{1/2} \leftrightarrow 2^2P_{1/2}$	121.5674	6.2649×10^8
$1 \leftrightarrow 2$	121.5670	4.6986×10^8

Table 2. Relevant parameters for the calculation of line escape factors Θ_L and their respective way of determination or used assumptions.

Parameter	Determination
Spatial H ($n = 1$) distribution	*Assumed* to be constant & equals to n_H
n_H	*Measured* via Balmer lines and Fulcher transition
Spatial H ($n = 2$) distribution	*Assumed* to follow n_e and T_e
$T_{H(n=2)}$ and $T_{H(n=1)}$	*Assumed* to be equal ($= T_H$)
T_H	*Measured* via TDLAS

Table 3. Wavelength and transition probabilities of the allowed dipole transitions between $n = 2$ and $n = 3$ states of atomic hydrogen (Balmer-α transition) [17].

Transition ($k \leftrightarrow i$)	Wavelength (nm)	A_{ik} (s^{-1})
$2^2P_{1/2} \leftrightarrow 3^2D_{3/2}$	656.2710	5.3877×10^7
$2^2S_{1/2} \leftrightarrow 3^2P_{3/2}$	656.2725	2.2448×10^7
$2^2P_{1/2} \leftrightarrow 3^2S_{1/2}$	656.2752	2.1046×10^6
$2^2S_{1/2} \leftrightarrow 3^2P_{1/2}$	656.2772	2.2449×10^7
$2^2P_{3/2} \leftrightarrow 3^2D_{5/2}$	656.2852	6.4651×10^7
$2^2P_{3/2} \leftrightarrow 3^2D_{3/2}$	656.2867	1.0775×10^7
$2^2P_{3/2} \leftrightarrow 3^2S_{1/2}$	656.2909	4.2097×10^6
$2 \leftrightarrow 3$	656.2819	4.4101×10^7

2.4. Tunable diode laser absorption spectroscopy

If a photon beam with the spectral radiant flux density $\Im_\lambda(\lambda, 0)$ hits a homogeneously absorbing plasma with the length l, $\Im_\lambda(\lambda, l)$ at the end of the plasma is given by the Lambert–Beer law [18]

$$\Im_\lambda(\lambda, l) = \Im_\lambda(\lambda, 0) \cdot \exp(-\kappa(\lambda) l). \quad (5)$$

In this case (i.e. the $n_{H(n=2)}$ determination), $\kappa(\lambda)$ corresponds to the H_α line absorption coefficient. It is given by the adaption of equation (4) to the H_α line.

Combining equation (5) and the expression for $\kappa(\lambda)$ while making use of the normalization condition of $P_{line}(\lambda)$ (i.e. $\int P_{line}(\lambda) d\lambda = 1$), an expression for $n_{H(n=2)}$ can be obtained. It is

$$n_{H(n=2)} = \frac{g_{n=2}}{g_{n=3}} \cdot \frac{8\pi c}{\lambda_{32}^4 l A_{32}} \cdot \int_{2\to3} \ln \frac{\Im_\lambda(\lambda, 0)}{\Im_\lambda(\lambda, l)} \, d\lambda. \quad (6)$$

It should be added, that the assumption of homogeneous absorption inside the plasma corresponds to a constant spatial $n_{H(n=2)}$ profile along the laser line of sight. As this is often not the case, the obtained $n_{H(n=2)}$ value after equation (6) should be treated as an average along the laser line of sight.

Considering the fine structure, the H_α line consists of seven transitions that are compiled in table 3. This table further shows the wavelength of the absorbed or emitted photons and the Einstein coefficient of each transition. The total H_α line profile is given by the sum of the seven individual line profiles while considering their relative intensities.

As pressure broadening can be neglected at the present pressure and n_e range, only natural broadening and Doppler broadening (depending on the H ($n = 2$) temperature $T_{H(n=2)}$) are considered as line broadening mechanisms. The line shape of one fine structure line is then given by the convolution of the Doppler (Gaussian) and naturally broadened (Lorentzian) line giving a Voigt profile. Its relative intensity is proportional to the product of the line's spontaneous emission Einstein coefficient and the degeneracy g_i of the respective upper fine structure level. This comes with the assumption of statistical equilibrium in the population of the $n = 2$ fine structure sub-levels resulting in a population of the sub-levels according to their statistical weights.

2.5. The TDLAS setup

The setup used for TDLAS measurements is based on a fibre coupled diode laser (*Sacher Lasertechnik*: TEC-500-0660-010) with 10 mW output power operated by using a Pilot PZ 0500 laser controller (*Sacher Lasertechnik*). By using the Littman–Metcalf principle [19] the laser has a wavelength tuning range from 652 nm to 660 nm. The H_α line profile is scanned temporally by applying a triangle voltage signal to a piezo element inside the laser head leading to a change in the length of the laser cavity. The spectral width of the emitted radiation is below 100 kHz (i.e. 0.14 fm at 656.28 nm) which is considerably smaller than the width of the H_α line profile. Thus, the emitted laser radiation is treated as monochromatic, i.e. the output voltage given by a photodiode illuminated with the laser is proportional to $\Im_\lambda$ of the laser radiation.

Using a fibre coupled beam splitter, the laser beam is split in two arms, one of which is used to irradiate the plasma. For acquisition of the transmitted laser intensity (i.e. $\Im_\lambda(\lambda, l)$ in equation (6)) a photodiode (*Thorlabs*: PDA36A-EC, gain: 1.5×10^3 V/A) equipped with an H_α interference filter. The measured voltage is denoted as U_{meas}. In the second arm, an H-K9L etalon (*Laser Components*: PP1037C, 15 pm free spectral range at 656 nm) is installed in the optical path to monitor the frequency variation of the laser photons. At the end of the beam path, the signal is measured by using another photodiode (gain: 1.5×10^4 V/A). The baseline signal $U_{baseline}$ (i.e. $\Im_\lambda(\lambda, 0)$ in equation (6)) is obtained by taking a reference measurement in the side arm simultaneously to the U_{meas} acquisition while having the etalon removed. For one spectrum measurement 100 spectra are taken and averaged to cancel any periodic noise and to enhance the signal-to-noise ratio.

An example for an obtained H_α spectrum is shown in figure 2 together with a simulation of the H_α line shape for $T_{H(n=2)} = 775$ K. Both profiles show excellent agreement which was also observed for all obtained spectra. From this match of measured and calculated line profiles one can

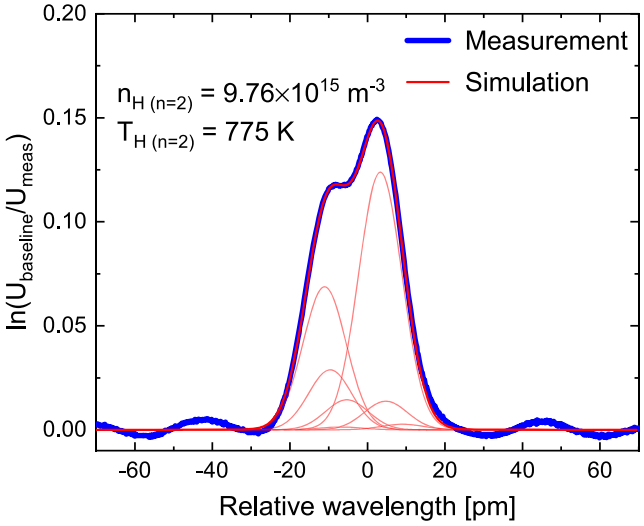

Figure 2. Logarithmic ratio of the baseline signal and U_{meas}. For comparison, a simulation of the H_α line profile for the temperature of 775 K is plotted.

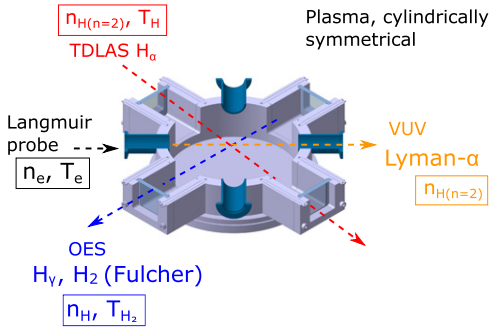

Figure 3. Lines of sight of the applied optical diagnostics and direction of the Langmuir probe pointing inside the planar ICP.

confirm the assumptions that were made for the line profile calculation. This holds especially for the population of the $n = 2$ fine structure sub-levels according to their statistical weights. However, the measured spectrum shows a sinusoidal behaviour in the parts off the line profile. This is attributed to some etalon effects remaining from the windows or inside the fibre optics. A possible way to prevent these oscillations is to use a signal measurement behind the plasma vessel without plasma operation as baseline. However, this raises high demands on the temporal stability during one measurement campaign which usually resembles a timescale of several hours. Unfortunately, this was not successful under the present conditions.

In order to determine $T_{\mathrm{H}(n=2)}$ inside the plasma, a least square fit of a theoretical line shape to the measured one is used whereas $n_{\mathrm{H}(n=2)}$ is obtained by integration of the curve in figure 2.

The TDLAS system was characterized with regard to possible effects which distort the TDLAS system. Regarding the H_α emission from the plasma causing an offset in the acquired signal U_{meas}, the influence on the obtained $n_{\mathrm{H}(n=2)}$ values was determined to be smaller than the error emerging from the measurement procedure. The influence of the $n = 2$ state depopulation process on the $n_{\mathrm{H}(n=2)}$ measurement was determined by measuring $n_{\mathrm{H}(n=2)}$ under varying laser power. Using the description of the process given by [20], the real density can be determined by extrapolation of the $n_{\mathrm{H}(n=2)}$ value to vanishing laser power. This procedure revealed a possible underestimation of the measured value of $n_{\mathrm{H}(n=2)}$ by roughly 15% under the standard conditions of the setup. This is connected to a value of the saturation parameter (after [21, 22]) of $S_0 = 0.33$. To obtain a higher signal-to-noise ratio, the laser power is not, however, reduced and the underestimation is assigned by an additional error bar.

The lines of sight of all used diagnostics can be seen in figure 3. Additionally, the measured quantities are denoted for each diagnostic. Since the antenna is cylindrically symmetrical and the diffusion of the plasma particles to the walls is isotropic in the radial direction, cylindrical symmetry is assumed for the plasma. Since the lines of sight for the optical diagnostics cross the plasma diagonally, they can therefore be assumed to be equivalent. From this can be concluded that the measurements that are performed via TDLAS and VUV emission spectroscopy can be compared directly.

3. Results

For the validation of the escape factor determination for Lyman-α emissivity correction two parameter scans of the pressure inside the vessel and the power coupled to the plasma were performed. One of those was performed under varying pressure between 2 Pa and 10 Pa while the power coupled to the plasma was kept constant at about 450 W. The other campaign was performed for a constant pressure of 5 Pa while the power coupled to the plasma increases from 360 W to 640 W.

3.1. General plasma parameters and Θ_{L} determination

Figures 4(a) and (b) show the T_{e} and n_{e} values measured at the center of the plasma vessel for the power variation and the pressure variation respectively. For both parameter scans, within their respective errors bars the behaviour of the measured values follows the expected behaviour, which means an almost constant T_{e} and rising n_{e} for an increase in power coupled to the plasma as well as a drop in T_{e} and a rise in n_{e} for increasing pressure [23]. In both scans, the value of T_{e} is between roughly 3 eV and 5 eV, whereas n_{e} is between 3×10^{16} m^{-3} and 5×10^{16} m^{-3}.

The hydrogen molecule temperature as well as $T_{\mathrm{H}(n=2)}$ can be seen in figures 5(a) and (b) for the power variation and the pressure variation respectively. Given the case that the population of H ($n = 2$) is dominated by excitation of atoms without kinetic energy gain (i.e. electron impact excitation and reabsorption of Lyman-α photons) the temperature of the $n = 2$ atoms resembles the temperature of H atoms in the ground state. This was confirmed for the investigated plasmas by the performed CR model calculations, which lead to the result that electron impact excitation accounts for more than 90% of the

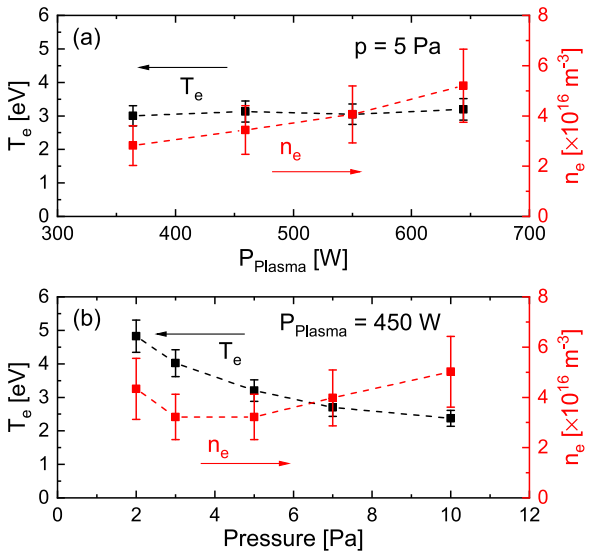

Figure 4. Electron temperature and density (a) for the power variation and (b) the pressure variation.

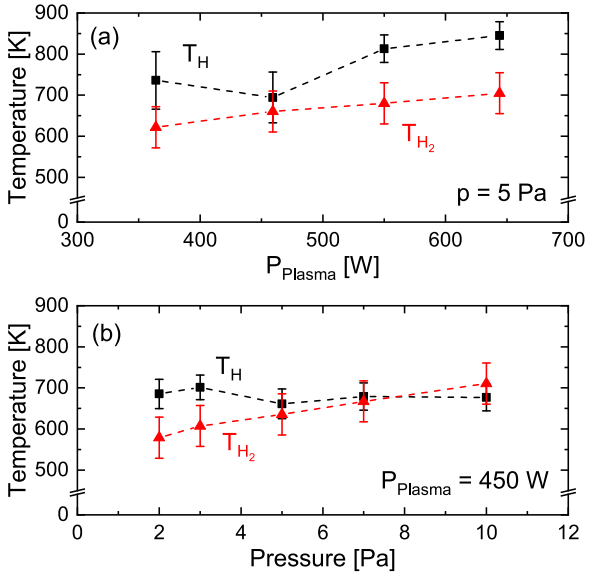

Figure 5. Hydrogen atom and molecule temperature (a) for the power variation and (b) the pressure variation.

H ($n = 2$) population. $T_{H(n=2)}$ is therefore depicted as T_H in figure 5.

For the power variation, both measured temperatures rise for increasing power values while the atomic temperature is above the molecular temperature. The rise of both temperatures is related to the increase of the electron density. This leads to an increasing frequency of inelastic collisions between electrons and neutral particles terminating in a higher kinetic energy transfer to the latter species. The higher value of T_H compared to T_{H_2} can be explained qualitatively as follows: in the course of the H atom production via electron impact dissociation, which is the main H atom production mechanism in the investigated plasmas, each produced atom gains the Franck–Condon-energy of up to 2 eV as kinetic energy (details

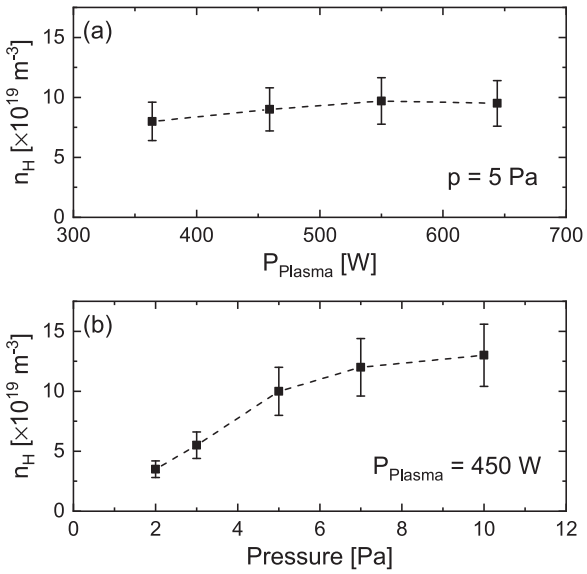

Figure 6. Hydrogen atom density (a) for the power variation and (b) the pressure variation.

can for example be found in [24]). This energy is transferred to the other heavy plasma particles by energy exchange collisions which ultimately leads to thermalization among all species if the collision rate is sufficient. However, for low pressure (and therefore low particle density), the rate of collisions between H atoms and molecules is not sufficient to lead to thermalization between the two species before the H atoms recombine at the vessel wall.

For the pressure variation, T_H is approximately constant at 680 K and lies above T_{H_2} for 2 Pa and 3 Pa being below 600 K. However, for rising pressure, the two temperatures agree within their error bars. This behaviour follows from the increasing particle densities and therefore increasing collisions between atoms and molecules leading to thermalization between the two species.

The n_H values measured during the power variation and the pressure variation are shown in figures 6(a) and (b) respectively. For an increase in power coupled to the plasma, n_H was found to increase slightly from 8×10^{19} m^{-3} to almost 1×10^{20} m^{-3}. This n_H rise may be connected to the increase in the electron density causing an enhancement of electron collisions with H_2 molecules leading to dissociation. For an increase in pressure, n_H was found to rise from 3.5×10^{19} m^{-3} to 1.3×10^{20} m^{-3}, which comes from the increase in the total amount of particles inside the plasma. For all investigated plasmas, the n_e and T_e results from the comparison to the Yacora H/H_2 data matched well with the values obtained via Langmuir probe.

Using all determined plasma parameters, the line escape factors Θ_L for correction of the Lyman-α emissivity can be calculated. The result of such a calculation is shown in figure 7 as a function of the hydrogen atom density for three different H atom temperature values. For the normalized spatial H ($n = 2$) density profile, a symmetric Bessel profile with the value 1 at the center and 0 at the edges was assumed. The line of sight is oriented perpendicular to the symmetry axis

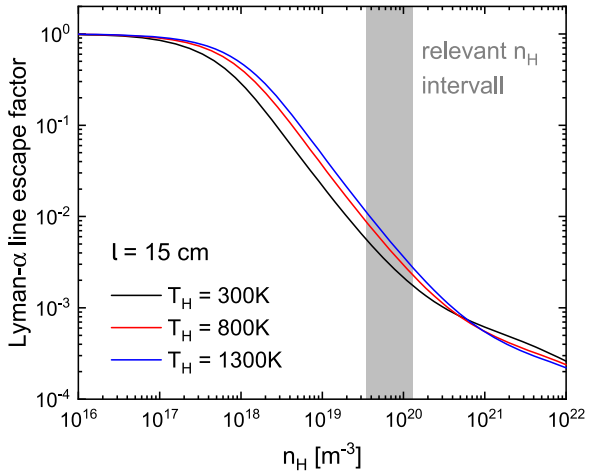

Figure 7. Line escape factors for the Lyman-α line calculated after [15] for varying T_H.

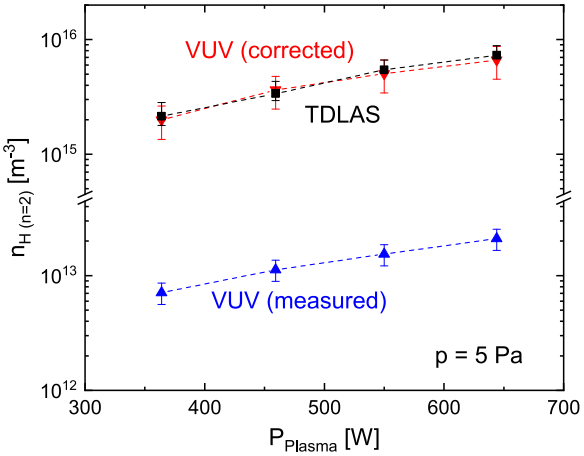

Figure 8. $n_{H(n=2)}$ measured by means of VUV emission spectroscopy both with and without (i.e. $\Theta_L = 1$) correction for self-absorption and TDLAS.

Table 4. Line escape factors (a) for the power variation and (b) the pressure variation.

(a)	For the power variation
P_{Plasma}	Θ_L $[\times 10^{-3}]$
360 W	$3.6^{+1.0}_{-0.6}$
460 W	$3.1^{+0.8}_{-0.5}$
550 W	$3.1^{+0.8}_{-0.6}$
640 W	$3.2^{+0.8}_{-0.6}$
(b)	For the pressure variation
p	Θ_L $[\times 10^{-3}]$
2 Pa	$8.2^{+2.4}_{-1.5}$
3 Pa	$5.1^{+1.4}_{-0.9}$
5 Pa	$2.8^{+0.7}_{-0.5}$
7 Pa	$2.3^{+0.6}_{-0.4}$

and has the length l of 15 cm corresponding to the diameter of the plasma vessel. Using the T_H and n_H values from figures 5 and 6 respectively, the Θ_L values for the Lyman-α emissivity correction are extracted from figure 7. They are collected in tables 4(a) and (b) together with their respective upper and lower error accounting for the uncertainty of the n_H and the T_H determination. This evaluation suggests that even at low n_H of slightly above 10^{19} m^{-3} a correction of the Lyman-α emissivity of 2 orders of magnitude is necessary to account for self-absorption.

3.2. Comparison between TDLAS and VUV emission spectroscopy—power variation

The $n_{H(n=2)}$ values measured by means of TDLAS and VUV emission spectroscopy are shown in figure 8. In the latter case, both the unprocessed (i.e. $\Theta_L = 1$, depicted as 'measured') and the datasets corrected of self-absorption are shown. The comparison between the TDLAS data and the unprocessed VUV emission spectroscopy data shows, that $n_{H(n=2)}$ is underestimated by roughly 2.5 orders of magnitude when determined with emission spectroscopy without any correction. The corrected data shows excellent agreement with TDLAS for each power value. The measurement error of the corrected VUV spectroscopy measurement is the combination of the error in the calibration factor (details can be found in [14]) and the Θ_L error. From this, the determined line escape factors are considered as reliable, despite accounting for a correction of orders of magnitude.

Figure 8 shows that $n_{H(n=2)}$ rises for increasing power coupled to the plasma. Since T_e was determined to be constant throughout the power variation, this behaviour arises from the increase in n_e and n_H causing an increase of the H ($n = 2$) formation via electron impact excitation of ground state H atoms. As already stated, this channel was found to be the main production channel of H ($n = 2$) atoms in the investigated plasmas.

3.3. Comparison between TDLAS and VUV emission spectroscopy—pressure variation

The corresponding graph for the pressure variation is shown in figure 9. Also here, the unprocessed VUV emission spectroscopy data is 2.5 orders of magnitude below the $n_{H(n=2)}$ values obtained by means of TDLAS. In addition, a very different pressure dependence is obtained from the TDLAS and the measured VUV emission spectroscopy data. While TDLAS suggests a $n_{H(n=2)}$ maximum for 5 Pa, the unprocessed emission spectroscopy data decreases continuously for rising pressure. With increasing pressure the atomic density and hence the self-absorption increases with the consequence that the line escape factor increases in this region by roughly an order of magnitude as well. That causes the deviation of the two diagnostics concerning the relative behaviour.

The corrected VUV emission spectroscopy values agree with the TDLAS measurement within their error bars. However, the relative $n_{H(n=2)}$ behaviour could still not be depicted correctly by using the escape factor correction. While

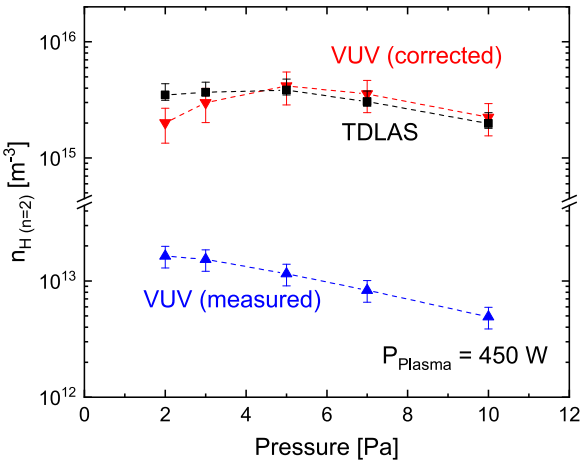

Figure 9. $n_{H(n=2)}$ measured by means of VUV emission spectroscopy both with and without (i.e. $\Theta_L = 1$) correction for self-absorption and TDLAS.

it matches with the TDLAS data for high pressure, the low pressure drop of $n_{H(n=2)}$ is overestimated by the corrected VUV emission spectroscopy. This behaviour might arise from changes of the spatial profiles of both emission and absorption of the Lyman-α photons for varying pressure. These changes are not considered in the escape factor calculations. Nevertheless, this measurement campaign underlines the reliability of the determined escape factors for the investigated set of H atom densities as input parameters. In addition, this measurement campaign shows, that the correction for self-absorption may not only be necessary to extract the absolute $n_{H(n=2)}$ values from the Lyman-α emissivity, but also to detect the right relative $n_{H(n=2)}$ behaviour.

The maximum of $n_{H(n=2)}$ is mainly determined by the interplay of n_H rising during the campaign and while T_e is decreasing affecting the H atom excitation rate into opposite directions, leading to a maximum in $n_{H(n=2)}$ for 5 Pa.

4. Conclusion

VUV emission spectroscopy measurements of the Lyman-α line are prone to photon self-absorption even in low pressure plasmas, which has been shown to lead to an underestimation of the H ($n = 2$) density by 2.5 orders of magnitude at H atom densities of 10^{19} m^{-3} to 10^{20} m^{-3}. After applying the determined line escape factors Θ_L, the VUV emission spectroscopy data shows good agreement with the data determined by TDLAS, which is known to be a reliable diagnostic. Θ_L was determined under various assumptions and depends mainly on the experimentally observed parameters n_H (via OES) and T_H (via TDLAS). The dedicated benchmark of the Θ_L determination with the TDLAS demonstrates that the applied method for the density correction for photon self-absorption can be considered as reliable in the full investigated parameter range, although there is some room for improvements concerning the spatial emission and absorption profiles of the Lyman-α photons.

Acknowledgments

This work has been carried out within the framework of the EUROfusion Consortium and has received funding from the Euratom research and training programme 2014-2018 and 2019-2020 under Grant agreement No. 633053. The views and opinions expressed herein do not necessarily reflect those of the European Commission.

ORCID iDs

F Merk https://orcid.org/0000-0002-0408-0832
R Friedl https://orcid.org/0000-0002-5723-994X
S Briefi https://orcid.org/0000-0003-2997-3503
U Fantz https://orcid.org/0000-0003-2239-3477

References

[1] Fantz U 2006 *Plasma Sources Sci. Technol.* **15** 137–47
[2] Wünderlich D and Fantz U 2016 *Atoms* **4** 26
[3] van Harskamp W E N, Brouwer C M, Schram D C, van de Sanden M C M and Engeln R 2011 *Phys. Rev.* E **83**036412
[4] van Harskamp W E N, Brouwer C M, Schram D C, van de Sanden M C M and Engeln R 2012 *Plasma Sources Sci. Technol.* **21** 024009
[5] Ladenburg R and Levy S 1930 *Z. Phys.* **65** 189–206
[6] Irons F E 1979 *J. Quant. Spectrosc. Radiat. Transfer* **22** 1–20
[7] Irons F E 1979 *J. Quant. Spectrosc. Radiat. Transfer* **22** 21–36
[8] Irons F E 1979 *J. Quant. Spectrosc. Radiat. Transfer* **22** 37–44
[9] Irons F E 1980 *J. Quant. Spectrosc. Radiat. Transfer* **24** 119–32
[10] Fantz U and Wimmer C 2011 *J. Phys. D: Appl. Phys.* **44** 335202
[11] Lackner M 2007 *Rev. Chem. Eng.* **23** 65–147
[12] Hopwood J 1994 *Plasma Sources Sci. Technol.* **3** 460
[13] Briefi S, Rauner D and Fantz U 2017 *J. Quant. Spectrosc. Radiat. Transfer* **187** 135–44
[14] Fröhler-Bachus C, Friedl R, Briefi S and Fantz U 2021 *J. Quant. Spectrosc. Radiat. Transfer* **259** 107427
[15] Behringer K 1998 *IPP Report 10/11* Max-Planck-Institut für Plasmaphysik, Garching, Germany https://pure.mpg.de/pubman/faces/ViewItemOverviewPage.jsp?itemId=item_2130808
[16] Thorne A P 1988 *Spectrophysics* (London: Chapman and Hall)
[17] Kramida A, Ralchenko Y and Reader J (The NIST ASD Team) 2020 *NIST Atomic Spectra Database* National Institute of Standards and Technology, Gaithersburg, USA *(Ver. 5.8)*
[18] Andrews D G 2010 *An Introduction to Atmospheric Physics* (Cambridge: Cambridge University Press)
[19] 2018 *Principles of Mode-Hop Free Wavelength Tuning* Sacher Lasertechnik GmbH Marburg, Deutschland http://docs.sacher-laser.com/pivotpoint.pdf
[20] Shimoda K 1983 *Introduction to Laser Physics* (Berlin: Springer)
[21] Demtröder W 2007 *Laserspektroskopie, Grundlagen und Techniken* (Berlin: Springer)
[22] Sadeghi N and Goto M 2020 *J. Quant. Spectrosc. Radiat. Transfer* **245** 106875
[23] Lieberman M A and Lichtenberg A J 2005 *Principles of Plasma Discharges and Materials Processing* (New York: Wiley)
[24] Celiberto R, Janev R K, Laricchiuta A, Capitelli M, Wadehra J M and Atems D E 2001 *At. Data Nucl. Data Tables* **77** 161–213